Journal of Catalysis **203,** 18–24 (2001)
doi:10.1006/jcat.2001.3313, available online at http://www.idealibrary.com on IDEAL®

Structural and Reactivity Properties of Nb–MCM-41: Comparison with That of Highly Dispersed Nb_2O_5/SiO_2 Catalysts

Xingtao Gao,* Israel E. Wachs,*,[1] Michael S. Wong,† and Jackie Y. Ying†

*Zettlemoyer Center for Surface Studies, Department of Chemical Engineering, Lehigh University, 7 Asa Drive, Bethlehem, Pennsylvania 18015; and †Department of Chemical Engineering, Massachusetts Institute of Technology, Room 66-544, Cambridge, Massachusetts 02139-4307

Received October 11, 2000; revised May 23, 2001; accepted May 30, 2001

The molecular structures of Nb cations in mesoporous material Nb–MCM-41 and the supported Nb_2O_5/SiO_2 catalyst under hydrated and dehydrated conditions were investigated by in-situ Raman and UV-vis-NIR diffuse reflectance spectroscopies. Methanol oxidation was employed as a chemical probe reaction to examine reactivity/selectivity properties of these catalytic materials. The structural characterization techniques demonstrate that similar surface Nb oxide species are present in both Nb–MCM-41 and Nb_2O_5/SiO_2 catalysts, which are sensitive to the environmental conditions (ambient or dehydrated). However, the characterization results also suggest that some Nb atoms in Nb–MCM-41 may be incorporated within the siliceous framework. The spectroscopic results revealed that under dehydrated conditions, the Nb cations in Nb–MCM-41 and 1% Nb_2O_5/SiO_2 are predominantly composed of isolated NbO_4 units, while the Nb cations in the supported Nb_2O_5/SiO_2 catalysts possess polymerized NbO_x species and/or bulk Nb_2O_5 with increasing Nb loading. The catalytic results indicate that the dispersed Nb cations in both types of catalysts are active redox sites for methanol oxidation and exhibit similar reactivity and selectivity properties due to the presence of Nb–O–Si bonds in their structures.

Key Words: **Nb–MCM-41; Nb_2O_5/SiO_2; catalysts; methanol oxidation; Raman spectroscopy; UV-visible diffuse reflectance spectroscopy.**

INTRODUCTION

Mesoporous materials (M41S) prepared through supramolecular templating have a highly defined mesopore structure and extremely large surface areas and have great potential as advanced catalytic materials for petroleum refining, partial oxidation, polymerization, pollution control, and enzyme and chiral chemistry (1–4). MCM-41, a member of the M41S family, possesses a hexagonal array of uniform mesopores that has recently attracted much attention (5). Isomorphous substitution of Si with other metal atoms in MCM-41 has been reported in the literature, such as Nb (2–4, 6), V (7–9), Mo (10), Cr (11), W (12), Sn (13), Ti (14, 15), and Zr (15). It has been shown that the local structure and bonding of MCM-41 materials are amorphous in nature, similar to amorphous silica (16). Consequently, it would be very interesting to compare the local structure of the metal atoms in the MCM-41 structure and on the surface of amorphous silica to better understand the catalytic behavior of the metal atom in different materials. In the present work, MCM-41 doped with Nb is compared to supported Nb_2O_5/SiO_2 catalysts.

The Nb_2O_5/SiO_2 supported catalysts have been examined for propylene photooxidation (17–20), partial oxidation of methane (21), and methanol oxidation (22). Nb(V) dispersed on silica exhibits redox characteristics rather than acidic characteristics (22). The local structure of the surface Nb(V) on silica has been extensively studied in the literature (17–24). It is generally accepted that at low Nb loadings, the dehydrated surface niobia species on silica predominantly consists of isolated NbO_4 species. Upon hydration, however, the coordination number of the surface niobia species may increase from four-fold to six-fold due to the adsorption and coordination of water molecules (19, 20). In contrast, the local structure of Nb(V) in MCM-41 has not been investigated in the literature. In the present work, the dispersion and local structures of niobia species in MCM-41 as well as on silica were investigated by Raman and UV-vis-NIR diffuse reflectance spectroscopies (DRS). The catalytic properties of these different Nb-Si materials were examined using methanol oxidation as a probe reaction. The comparative structural and reactivity studies of these two catalyst systems will provide a better understanding of the relationship between the structural characteristics and the reactivity/selectivity properties of these Nb–Si-based catalytic materials.

EXPERIMENTAL

Synthesis of Pure and Nb-Doped MCM-41

The preparation of Nb-doped MCM-41 was based on the synthesis procedures of Zhang and Ying (3). A solution

---

[1] To whom correspondence should be addressed. Fax: (610)-758-6555. E-mail: iew0@lehigh.edu.

0021-9517/01 $35.00

of tetramethylammonium silicate (10 wt% SiO_2, Sachem) was combined with a 7.8 wt% solution of cetyltrmethylammonium bromide (Aldrich) such that the Si/surfactant molar ratio was 7.5. Niobium ethoxide (Strem) was added to the stirring white, viscous mixture to give a Nb–Si dopant precursor molar ratio of 28.1. The pH was adjusted to 11 with concentrated H_2SO_4, and the mixture was stirred for an additional 1.5 h at room temperature. The pH rose during the stirring and was adjusted back to pH 11. After 0.5 h of further stirring, the mixture was placed in several Teflon-sealed glass tubes and aged at 100°C in a heated silicone oil bath for 7 days. A white precipitate was recovered, washed with 3 aliquots of water, and left to dry overnight. Finally, the dried powder was calcined at 650°C for 6 h in a static box furnace. Bulk elemental analysis was accomplished by QTI (Whitehouse, NJ), and 3.5 wt% Nb was found in Nb–MCM-41. The preparation of undoped MCM-41 was carried out in a similar manner. The Nb precursor was excluded from the synthesis mixture and the resulting as-synthesized material was calcined at 600°C.

Synthesis of Nb_2O_5/SiO_2 Supported Oxide Catalysts

The silica support used was Cabosil EH-5 (S_{BET} = 332 m^2/g). The Nb_2O_5/SiO_2 catalysts were prepared by the nonaqueous impregnation method employing niobium ethoxide precursor, as described in detail elsewhere (24). The preparation was performed inside a glove box with continuously flowing N_2. After impregnation, the samples were kept inside the glove box with flowing N_2 overnight. The samples were subsequently dried in flowing N_2 at 120°C for 1 h and 300°C for 1 h. Then, the samples were calcined in flowing air at 300°C for 1 h and 500°C for 2 h. The 15 wt% Nb_2O_5 loading sample was prepared by repeating the impregnation procedure on calcined 10% Nb_2O_5/SiO_2 as the starting material.

Mesostructure Characterization

Powder X-ray diffraction (XRD) data were recorded on a Siemens D5000 diffractometer operated at 45 kV and 40 mA, using nickel-filtered CuK_α radiation with a wavelength of 1.5406 Å. Nitrogen adsorption isotherms were obtained at 77 K on a Micromeritics ASAP 2010 Gas Sorption and Porosimetry System. Samples were degassed at 150°C under vacuum until a final pressure of 1×10^{-3} Torr was reached. Brunauer–Emmett–Teller surface areas were determined over a relative pressure range from 0.05 to 0.20. Pore size distributions were calculated from the adsorption branch of the isotherms using the Barrett–Joyner–Halenda method.

Raman Spectroscopy

The Raman spectra were obtained with the 514.5 nm line of an Ar^+ ion laser (Spectra Physics, Model 164). The scattered radiation from the sample was directed into an OMA III (Princeton Applied Research, Model 1463) optical multichannel analyzer with a photodiode array cooled thermoelectrically to −35°C. The samples were pressed into self-supporting wafers. The Raman spectra of the hydrated samples were taken during sample spinning under ambient conditions. The Raman spectra of the dehydrated samples were recorded at room temperature after heating the sample in flowing O_2 at 450–500°C for 1 h in a stationary quartz cell.

UV-vis-NIR Diffuse Reflectance Spectroscopy

The DRS experiments were conducted on Varian Cary 5E UV-vis-NIR spectrophotometer with the integration sphere diffuse reflectance attachment. The DRS spectra were processed with Bio-Rad Win-IR software, consisting of calculation of $F(R_\infty)$ from the absorbance. The edge energy (E_g) for allowed transitions was determined by finding the intercept of the straight line in the low energy rise of a plot of $[F(R_\infty) \times h\nu]^2$ against $h\nu$, where $h\nu$ is the incident photon energy (38). The samples were loaded in a quartz flow cell with a Suprasil window and were measured in the region of 200–2200 nm at room temperature. A halon white (PTFE) reflectance standard was used as the baseline unless otherwise noted. The spectra of hydrated samples were obtained under ambient conditions. The spectra of the dehydrated samples were obtained after the samples were calcined at 500°C in flowing O_2/He for 1 h.

In order to minimize the possible effect of regular reflection introduced by the high concentrations of Nb cations, the samples were diluted with non- or weak-absorbing white materials of SiO_2 or MCM-41. Nb–MCM-41 was diluted with MCM-41. The Nb_2O_5/SiO_2 catalysts and the Nb-containing reference oxides/compounds were diluted with pure SiO_2. The amount of diluent used for a sample depends on the absorbance of the sample, which needs to result in the Kubelka–Munk function $F(R_\infty) \sim 1$ or less after diluting. The corresponding diluent was also used as the baseline standard. For the NIR experiments, however, only pure samples were used.

Methanol Oxidation

Methanol oxidation was used to examine the catalytic properties of the Nb–MCM-41 and Nb_2O_5/SiO_2 samples. The reaction was carried out in an isothermal fixed-bed differential reactor. About 60 mg of catalyst, with a size fraction of 60–100 mesh, was tested for methanol oxidation at atmospheric pressure. The samples were pretreated in a stream of O_2/He gas mixture at 450°C for 0.5 h before each run. The reactant gas mixture of CH_3OH/O_2/He, molar ratio of ∼6/13/81, was used with a total flow rate of 100 ml/min. The overall conversion of methanol was kept below 10%. Analysis of the reactor effluent was performed using an online gas chromatograph (HP 5890 Series II) equipped with FID and TCD detectors. A Carboxene-1000 packed column and a CP-Sil 5CB capillary column were used in parallel for TCD and FID, respectively.

RESULTS AND DISCUSSION

Mesostructure of Nb–MCM-41 and Nb_2O_5/SiO_2

The XRD patterns of the calcined MCM-41 and Nb–MCM-41 are shown in Fig. 1. The diffraction pattern for these materials is characteristic of MCM-41 materials, indicative of the highly ordered hexagonal packing of the pores (1–4). Such an ordered mesostructure does not exist in the supported oxide materials. The N_2 adsorption isotherm of Nb–MCM-41 shown in Fig. 2 is a Type-IV isotherm, typical of the MCM-41 mesoporous structure (1–4). For comparison, the N_2 isotherms for the 1 and 10% Nb_2O_5/SiO_2 samples are also presented in Fig. 2.

The mesostructural properties of Nb–MCM-41 and Nb_2O_5/SiO_2 samples are listed in Table 1. The pore size distributions for Nb–MCM-41 are very different from those of the 1 and 10% Nb_2O_5/SiO_2 samples (not shown here). Nb–MCM-41 exhibits a much smaller pore size and a narrower pore size distribution than the supported oxide materials. 1 and 10% Nb_2O_5/SiO_2 samples have larger mesopores with a broad size distribution (28). The N_2 isotherms of the supported oxides resemble Type IV more than Type II isotherms (Fig. 2), suggesting that the mesopores are internal to the supported oxide particles and do not represent interparticle porosity.

Raman Spectroscopy

The Raman spectra of the dehydrated MCM-41, Nb–MCM-41, SiO_2, and 10% Nb_2O_5/SiO_2 samples are presented in Fig. 3. MCM-41 exhibits Raman bands at 973,

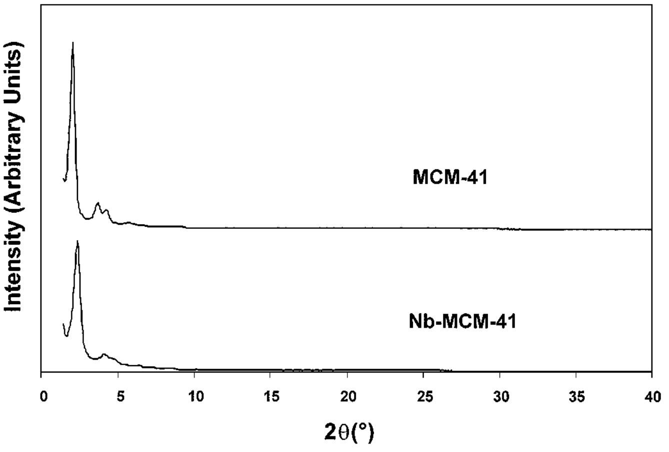

FIG. 1. XRD patterns of calcined MCM-41 and Nb–MCM-41 samples.

TABLE 1

Mesostructural Characteristics of MCM-41, Nb–MCM-41, and Supported Nb_2O_5/SiO_2 Catalysts

Sample	Surface area (cm^2/g)	Pore vol. (cm^3/g)	Avg. pore dia. (Å)	Unit cell (a_0) (Å)
MCM-41	987.0	0.70	26.9	49.0
Nb–MCM-41	951.5	0.53	24.1	42.4
1% Nb_2O_5/SiO_2	269.6	1.43	~500	—
10% Nb_2O_5/SiO_2	295.3	1.24	~360	—

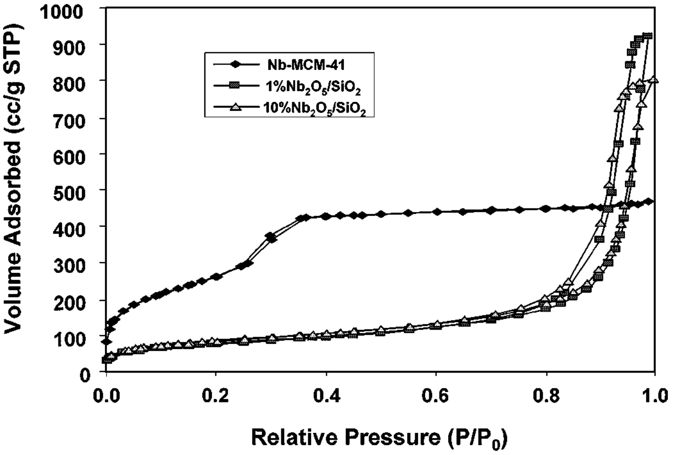

FIG. 2. N_2 adsorption isotherms of Nb–MCM-41, 1% Nb_2O_5/SiO_2, and 10% Nb_2O_5/SiO_2.

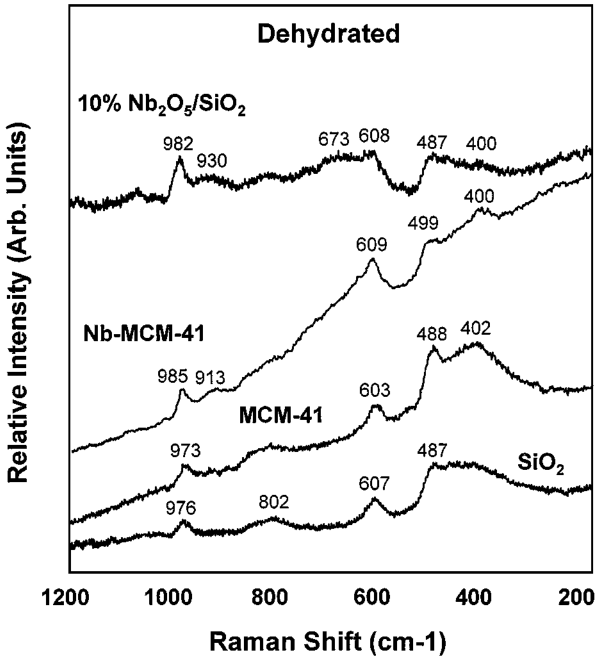

FIG. 3. Raman spectra of the dehydrated MCM-41, Nb–MCM-41, SiO_2, and 10% Nb_2O_5/SiO_2 samples.

~815, 603, ~488, and ~402 cm^{-1}, which are very similar to the vibrations of the amorphous SiO_2 support. This result is consistent with previous literature (16). For amorphous SiO_2, the ~976 cm^{-1} band is associated with the Si–OH stretching mode of the surface hydroxyls (28), and the bands at ~802 and 410–430 cm^{-1} have been assigned to the Si–O–Si symmetrical stretching and bending modes, respectively (31). The broad bands at 607 and 487 cm^{-1} have been assigned to D2 and D1 defect modes that are attributed to tri- and tetra-cyclosiloxane rings, respectively (31, 32). For the dehydrated 10% Nb_2O_5/SiO_2 sample, the 982 cm^{-1} band has been assigned to the Nb=O stretching mode of isolated surface NbO_4 species (26). A weak Raman band was also observed at ~673 cm^{-1} due to bulk Nb_2O_5 (33, 34), indicative of the presence of some Nb_2O_5 crystallites on silica at this high loading. The broad, weak band at ~930 cm^{-1}, which is also observed for other surface metal oxide species on silica (e.g., V(V), Ti(IV), and Mo(VI)) and is not a function of the metal oxide loading, has been assigned to $Si(-O^-)/Si(-O^-)_2$ functionality due to the formation of M–O–Si bonds (35, 36). However, the presence of surface polymerized niobia species, which exhibit Raman bands in the 823–935 cm^{-1} region (26), cannot be excluded. For the dehydrated Nb–MCM-41 sample, the new Raman band at ~985 cm^{-1} should also be assigned to the Nb=O stretching mode of isolated NbO_4 species. The Raman bands at 609, 499, and 400 cm^{-1} appear to be due to the amorphous-type silica vibrations.

The Raman spectra of MCM-41, Nb–MCM-41, and 10% Nb_2O_5/SiO_2 samples under ambient conditions (hydrated) are presented in Fig. 4. No appreciable change was observed for MCM-41 upon hydration, similar to amorphous SiO_2. For the hydrated 10% Nb_2O_5/SiO_2 sample, broad Raman bands are observed at ~920, ~810, ~673, 613, and 486 cm^{-1}. These bands are very similar to the Raman bands observed for amorphous $Nb_2O_5 \cdot nH_2O$ (33, 34), indicating the presence of a similar type of hydrated surface niobia species. The Raman band at ~920 cm^{-1} is associated with the terminal Nb=O surface sites on this type of surface, amorphous $Nb_2O_5 \cdot nH_2O$ species (33). The NbO_6 units of the surface hydrated niobia species on silica might be connected by Nb–OH–Nb bridges, as in the case of the fully hydrated vanadium oxide species on silica that resembles $V_2O_5 \cdot nH_2O$ gels (35), since the structures of the surface niobia species are reversible during hydration and dehydration. The Raman spectrum of the hydrated Nb–MCM-41 is very similar to that of the hydrated 10% Nb_2O_5/SiO_2 sample, suggesting the presence of surface hydrated $Nb_2O_5 \cdot nH_2O$ species. The shoulder at ~982 cm^{-1} may be due to the remaining isolated NbO_4 species. This result suggests the possible presence of two types of Nb species: one is the surface type that forms hydrated, polymerized niobium oxide species and the other one is the framework type that does not polymerize upon hydration. The Raman spectrum of the Nb incorporated silicate of the MFI structure has been reported (37). Unfortunately, the Raman spectrum shown is not very clear and no useful information is given about the vibrations of framework Nb cations. For other metal incorporated MCM-41 materials, such as V(V) (7) and Cr(VI) (11), the Raman spectra shown reflect the presence of surface metal oxide species on the MCM-41 surface. The Raman signal regarding the incorporated metal cations in MCM-41 may be weak and covered by the strong signal from the surface metal oxide species.

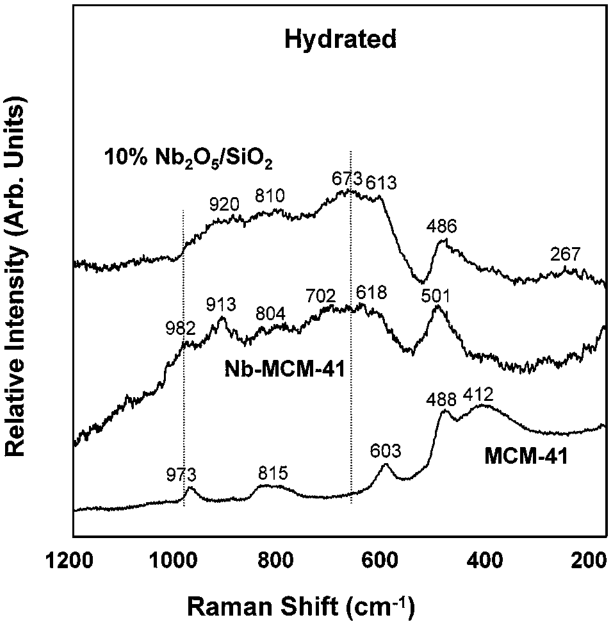

FIG. 4. Raman spectra of the hydrated MCM-41, Nb–MCM-41, and 10% Nb_2O_5/SiO_2 samples.

UV-vis-NIR Diffuse Reflectance Spectroscopy

The NIR–DR spectra of the dehydrated MCM-41, Nb–MCM-41, SiO_2, and 1–15% Nb_2O_5/SiO_2 samples are shown in Fig. 5. Both types of materials exhibit the same band at 7318 cm^{-1} due to the 2ν overtone vibration of isolated Si–OH hydroxyls (39). It is noted that the 7318 cm^{-1} band for the Nb_2O_5/SiO_2 samples decreases upon increasing niobia loading, indicating that deposition of niobium oxide species on SiO_2 consumes surface Si–OH hydroxyls. In contrast, the intensity/surface area of the 7318 cm^{-1} band for Nb–MCM-41 and MCM-41 is about the same, indicating that the presence of Nb in MCM-41 does not affect the Si–OH hydroxyl concentration. This result suggests that the incorporation of Nb is not associated with anchoring Nb atoms via the surface Si–OH hydroxyls of MCM-41 but rather incorporating into the MCM-41 framework and/or binding to the MCM-41 wall surface simultaneously at the formation of the Nb–MCM-41 structure. Interestingly,

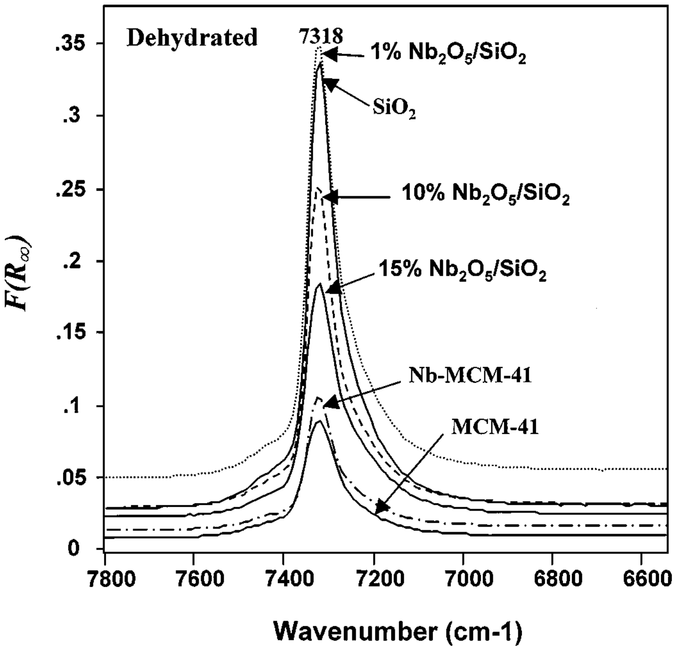

FIG. 5. NIR–DRS spectra of MCM-41, Nb–MCM-41, SiO_2, and 1, 10, and 15% Nb_2O_5/SiO_2 under dehydrated conditions.

the much lower intensity of Si–OH hydroxyl band at 7318 cm^{-1} of MCM-41 relative to amorphous SiO_2 indicates that MCM-41 materials possess a lower hydroxyl concentration than amorphous silica, suggesting that MCM-41 materials are more hydrophobic than amorphous silica and silica-supported niobia amorphous materials.

The UV-vis-DR spectra of some Nb-reference compounds are shown in Fig. 6, and their edge energies are listed in Table 2. It is noted that the increase of the NbO_6 structural distortion from $KNbO_3$, $NaNbO_3$ to $LiNbO_3$ increases the edge energy from 3.39 to 3.89 eV. The decrease of the layer thickness of the layered oxide compounds ($KCa_2Na_2Nb_5O_{16}$, $KCa_2NaNb_4O_{13}$, and $KCa_2Nb_3O_{10}$) slightly increases the edge energy from 3.42 to 3.57 eV. All the above Nb oxide compounds possess polymerized NbO_6 structures with five or six Nb–O–Nb bonds around the central Nb cation (33). Unfortunately, it is difficult to find a wide variety of Nb-reference compounds with completely different structures to establish a reliable correlation between structure and edge energy, as in the case of the V-reference compounds (42). Nevertheless, the results indicate that the Nb oxide compounds with polymerized NbO_x structure exhibit edge energies below 3.9 eV.

TABLE 2

Edge Energies of Nb-Containing Oxides/Compounds and Catalysts

Sample	E_g (eV) (hydrated)	E_g (eV) (dehydrated)	Structural assignments[a]
$LiNbO_3$	3.89	—	polymerized NbO_6
$NaNbO_3$	3.51	—	polymerized NbO_6
$KNbO_3$	3.39	—	polymerized NbO_6
Nb_2O_5	3.42	—	polymerized $NbO_{6,7,8}$
$KCa_2Na_2Nb_5O_{16}$	3.42	—	polymerized NbO_6
$KCa_2NaNb_4O_{13}$	3.47	—	polymerized NbO_6
$KCa_2Nb_3O_{10}$	3.57	—	polymerized NbO_6
$YbNbO_4$	3.13	—	polymerized NbO_4
1% Nb_2O_5/SiO_2	4.34	4.37	isolated NbO_4
10% Nb_2O_5/SiO_2	3.92	3.92	isolated NbO_4 + polymerized NbO_x
Nb–MCM41	4.43	4.46	isolated NbO_4

[a] Structural assignments for Nb-reference compounds can be found in (33) and references herein.

The UV-vis-DR spectra of the MCM-41, Nb–MCM-41, and 1 and 10% Nb_2O_5/SiO_2 samples under hydrated and dehydrated conditions are shown in Fig. 7. The corresponding edge energies are also listed in Table 2. No noticeable

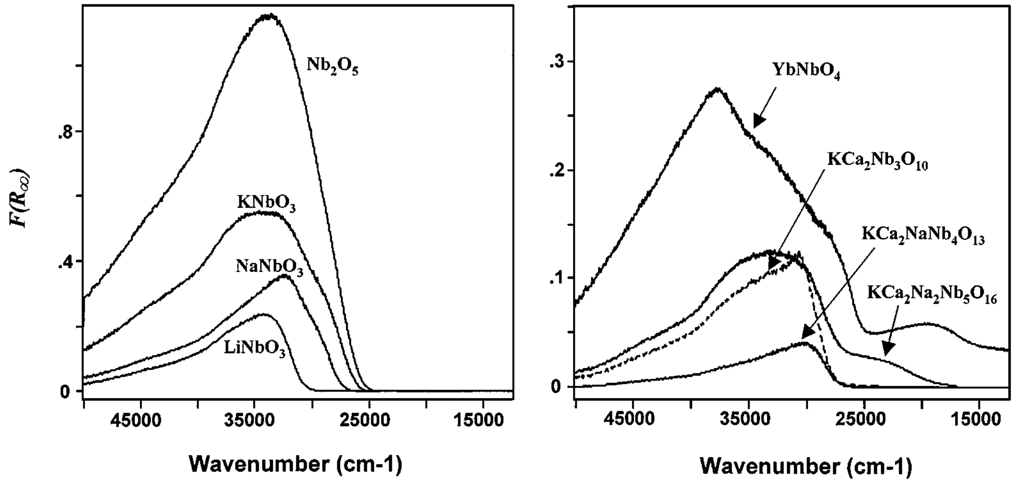

FIG. 6. UV-vis-DRS spectra of Nb-containing reference oxides/compounds.

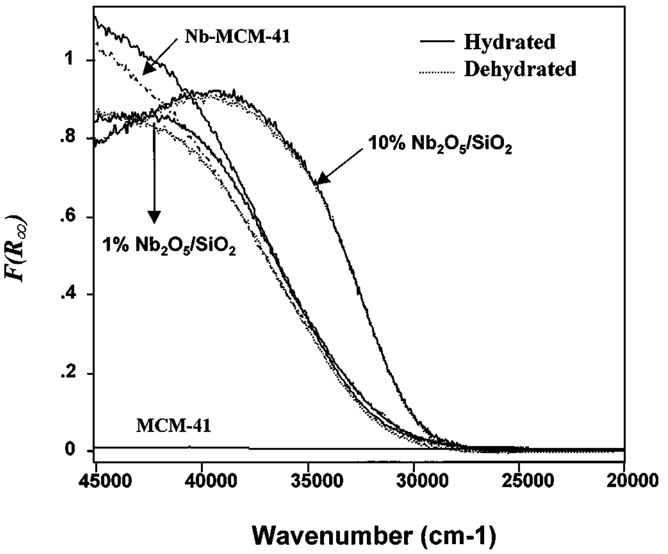

FIG. 7. UV-vis-DRS spectra of MCM-41, Nb–MCM-41, and 1 and 10% Nb_2O_5/SiO_2 under hydrated and dehydrated conditions.

absorption in the UV-vis region is observed for MCM-41, similar to amorphous SiO_2 (39). For Nb–MCM-41 and Nb_2O_5/SiO_2, the LMCT transitions of Nb cations are observed above 30,000 cm^{-1}. As seen from Fig. 7, the intensity of the LMCT transitions of Nb cations on the hydrated Nb–MCM-41 and 1% Nb_2O_5/SiO_2 samples decreases upon dehydration, suggesting ligand changes around the Nb cations upon hydration/dehydration. In contrast, no significant spectral change is observed for the 10% Nb_2O_5/SiO_2 sample upon hydration/dehydration. The E_g values shown in Table 2 for the hydrated Nb–MCM-41 and 1% Nb_2O_5/SiO_2 samples are 4.43 and 4.34 eV, respectively. These E_g values are significantly higher than the Nb-reference compounds with polymerized NbO_x units, suggesting that the hydrated Nb–MCM-41 and 1% Nb_2O_5/SiO_2 samples possess very small $Nb_2O_5 \cdot nH_2O$ clusters. Dehydration only results in a minor increase of the edge energy by 0.03 eV. The slight increase of edge energies for Nb–MCM-41 and 1% Nb_2O_5/SiO_2 upon dehydration may be associated with a decrease in cluster sizes as well as the ligand changes around Nb cations. This suggests the presence of isolated NbO_4 species, which is consistent with the Raman results. The lower E_g value of 3.92 eV for 10% Nb_2O_5/SiO_2 in both hydrated and dehydrated states is consistent with the Raman results, which suggests that the niobia species are dominant in polymerized species and/or bulk niobia since polymerized NbO_x units and bulk niobia possess edge energies below 3.9 eV.

Methanol Oxidation

The catalytic results of Nb–MCM-41 and dispersed Nb_2O_5/SiO_2 catalysts for methanol oxidation at 250°C are presented in Table 3. MCM-41 and SiO_2 showed no noticeable activity. The Nb–MCM-41 and 1% Nb_2O_5/SiO_2 samples with predominantly isolated NbO_4 species produce exclusively redox products and show similar reactivity (TOFs), indicating that isolated Nb cations are the active redox sites for methanol oxidation over these different types of materials. This result further confirms that both Nb–MCM-41 and Nb_2O_5/SiO_2 at a low niobia loading only possess weak Lewis acid sites (5, 40). For the 10 and 15% Nb_2O_5/SiO_2 samples that possess isolated NbO_4 and bulk niobia and/or polymerized species, a small amount of dimethyl ether is obtained in addition to the redox products. The production of dimethyl ether must come from the Brønsted acid sites that are associated with bulk niobia at high niobia loadings (40). Furthermore, their reactivity (TOFs) decreases dramatically as compared to the 1% Nb_2O_5/SiO_2 sample, suggesting that these samples possess a significant amount of polymerized niobia species and/or bulk niobia since bulk niobia is much less active than the isolated NbO_4 species (22). Nb–MCM-41 and dispersed Nb_2O_5/SiO_2 catalysts exhibit similar selectivities, suggesting they have active sites common to both systems, namely the isolated NbO_4 surface sites with Nb–O–Si bonds. It is noted that the 1% Nb_2O_5/SiO_2 sample exhibits a higher selectivity to methyl formate (at 67%) than the rest of the catalysts at the present conditions. This may be due to its relatively high surface methoxy concentration originated from a low methanol conversion ($A_c = 8$ mmol/g · h) and a high Si–OH concentration as demonstrated by the NIR–DRS experiment (Fig. 5). At a higher methanol conversion ($A_c = 19$ mmol/g · h) at 270°C, the HCHO selectivity for 1% Nb_2O_5/SiO_2 reaches 49% and the selectivity of methyl formate decreases to 45%.

In addition, the activation energies (E_a) of the Nb–MCM-41 and 1 and 10% Nb_2O_5/SiO_2 samples for methanol oxidation are 19.6, 23.7, and 21.5 kcal/mol, respectively, which are typical for methanol oxidation over transition-metal

TABLE 3

Activity/Selectivity of Nb–MCM-41 and Nb_2O_5/SiO_2 Catalysts for Methanol Oxidation at 250°C

Catalyst	A_c^a (mmol/g · h)	TOF[b] (10^{-3} s^{-1})	Selectivity (%) HCHO	MF	DMM	DME
Nb–MCM-41	27	20	52	44	4	0
1% Nb_2O_5/SiO_2	8	29	27	67	6	0
10% Nb_2O_5/SiO_2	21	7	57	32	6	5
15% Nb_2O_5/SiO_2	17	4	60	23	8	9

[a] Millimoles of methanol converted per gram catalyst per hour.

[b] TOF is calculated on the basis of the total Nb atoms in the catalyst for the production of HCHO (formaldehyde) + MF (methyl formate) + DMM (dimethoxy methane).

oxide catalysts (41). This further confirms that the dispersed Nb cations are the active sites for methanol oxidation over these Nb-containing silica catalysts.

CONCLUSIONS

Similar surface Nb species are present in both Nb–MCM-41 and Nb_2O_5/SiO_2 catalysts, which are sensitive to the environmental conditions (ambient or dehydrated). Some Nb atoms in the Nb–MCM-41 sample may be incorporated into the siliceous framework. The results revealed that the Nb cations in Nb–MCM-41 and 1% Nb_2O_5/SiO_2 are predominantly isolated NbO_4 species under dehydrated conditions, while polymerized surface niobia species and/or bulk Nb_2O_5 are formed at high Nb loadings on SiO_2. The catalytic results indicate that the dispersed Nb cations in both types of catalysts are active redox sites for methanol oxidation. The Nb–MCM-41 and 1% Nb_2O_5/SiO_2 have similar reactivity/selectivity properties of their active sites, but Nb–MCM-41 has a higher overall activity due to the greater amount of isolated NbO_4 species per unit mass catalyst. In addition, Nb–MCM-41 is more hydrophobic due to its lower surface Si–OH concentration as compared to the silica-supported niobia amorphous materials.

ACKNOWLEDGMENTS

This work was supported by the U.S. Department of Energy—Basic Energy Sciences, Grant DE-FG02-93ER14350. The authors are grateful for the donation of some of the Nb-reference compounds by Prof. Tsunehiro Tanaka (Kyoto University, Japan).

REFERENCES

1. Biz, S., and Occelli, M. L., *Catal. Rev. Sci. Eng.* **40**, 329 (1998).
2. Ying, J. Y., Mehnert, C. P., and Wong, M. S., *Angew. Chem. Int. Ed.* **38**, 56 (1999).
3. Zhang, L., and Ying, J. Y., *AIChE J.* **43**, 2793 (1997).
4. Antonelli, D. M., and Ying, J. K., *Angew. Chem. Int. Ed. Engl.* **35**, 426 (1996).
5. Kresge, C. T., Leonowicz, M. E., Roth, W. J., Vartuli, J. C., and Beck, J. S., *Nature* **359**, 710 (1992).
6. Ziolek, M., Nowak, I., and Lavalley, J. C., *Catal. Lett.* **45**, 259 (1997).
7. Chao, K. J., Wu, C. N., Chang, H., Lee, L. J., and Hu, S., *J. Phys. Chem. B* **101**, 6341 (1997).
8. Wei, D., Wang, H., Feng, X., Chueh, W.-T., Ravikovitch, P., Lyubovsky, M., Li, C., Takeguchi, T., and Haller, G. L., *J. Phys. Chem. B* **103**, 2113 (1999).
9. Chatterjee, M., Iwasaki, T., Hayashi, H., Onodera, Y., Ebina, T., and Nagase, T., *Chem. Mater.* **11**, 1368 (1999).
10. Rana, R. K., and Viswanathan, B., *Catal. Lett.* **52**, 25 (1998).
11. Zhu, Z., Chang, Z., and Kevan, L., *J. Phys. Chem. B* **103**, 2680 (1999).
12. Zhang, Z., Suo, J., Zhang, X., and Li, S., *Appl. Catal. A: General* **179**, 11 (1999).
13. Chaudhari, K., Das, T. K., Rajmohanan, P. R., Lazar, K., Sivasanker, S., and Chandwadkar, A. J., *J. Catal.* **183**, 281 (1999).
14. Corma, A., Navarro, M. T., and Perez Pariente, J., *J. Chem. Soc. Chem. Commun.* 147 (1994).
15. Occelli, M. L., Biz, S., and Auroux, A., *Appl. Catal. A: General* **183**, 231 (1999).
16. Chen, C.-Y., Li, H.-X., and Davis, M. E., *Micropor. Mater.* **2**, 17 (1993).
17. Tanaka, T., Nojima, H., Yoshida, H., Nakagawa, H., Funabiki, T., and Yoshida, S., *Catal. Today* **16**, 297 (1993).
18. Yoshida, S., Nishimura, Y., Tanaka, T., Kanai, H., and Funabiki, T., *Catal. Today* **8**, 67 (1990).
19. Yoshida, H., Tanaka, T., Yoshida, T., Funabiki, T., and Yoshida, S., *Catal. Today* **28**, 79 (1996).
20. Yoshida, S., Tanaka, T., Hanada, T., Hiraiwa, T., Kanai, H., and Funabiki, T., *Catal. Lett.* **12**, 277 (1992).
21. Arena, F., Frusteri, F., Parmaliana, A., and Giordano, N., *J. Catal.* **143**, 299 (1993).
22. Wachs, I. E., Jehng, J.-M., Deo, G., Hu, H., and Arora, N., *Catal. Today* **28**, 199 (1996).
23. Jehng, J.-M., Hu, H., Gao, X., and Wachs, I. E., *Catal. Today* **28**, 335 (1996).
24. Jehng, J.-M., and Wachs, I. E., *J. Phys. Chem.* **95**, 7373 (1991).
25. Jehng, J.-M., and Wachs, I. E., *J. Mol. Catal.* **67**, 369 (1991).
26. Burcham, L. J., Datka, J., and Wachs, I. E., *J. Phys. Chem. B* **103**, 6015 (1999).
27. Gregg, S. J., and Sing, K. S. W., “Adsorption, Surface Area and Porosity,” 2nd ed. Academic Press, New York, 1982.
28. Tallant, D. R., Bunker, B. C., Brinker, C. J., and Balfe, C. A., *Mater. Res. Soc. Symp. Proc.* **73**, 261 (1986).
29. Stolen, R. H., and Walrafen, G. E., *J. Chem. Phys.* **64**, 2623 (1976).
30. Brinker, C. J., Tallant, D. R., Roth, E. P., and Ashley, C. S., *Mater. Res. Soc. Symp. Proc.* **61**, 387 (1986).
31. Brinker, C. J., Kirkpatrick, R. J., Tallant, D. R., Bunker, B. C., and Montez, B., *J. Non-Cryst. Solids* **99**, 418 (1988).
32. Morrow, B. A., and McFarlan, A. J., *J. Non-Cryst. Sol.* **120**, 61 (1990).
33. Jehng, J.-M., and Wachs, I. E., *Chem. Mater.* **3**, 100 (1991). [references therein]
34. Maurer, S. M., and Ko, E. I., *J. Catal.* **135**, 125 (1992).
35. Gao, X., Bare, S. R., Weckhuysen, B. M., and Wachs, I. E., *J. Phys. Chem. B* **102**, 10,842 (1998).
36. Deo, G., Turek, A. M., Wachs, I. E., Huybrechts, D. R. C., and Jacobs, P. A., *Zeolites* **13**, 365 (1993).
37. Prakash, A. M., and Kevan, L., *J. Am. Chem. Soc.* **120**, 13,148 (1998).
38. Delgass, W. N., Haller, G. L., Kellerman, R., and Lunsford, J. H., “Spectroscopy in Heterogenous Catalysis,” p. 86. Academic Press, New York, 1979.
39. Gao, X., Bare, S. R., Fierro, J. L. G., Banares, M. A., and Wachs, I. E., *J. Phys. Chem. B* **102**, 5653 (1998).
40. Datka, J., Turek, A. M., Jehng, J. M., and Wachs, I. E., *J. Catal.* **135**, 186 (1992).
41. Weber, R. S., *J. Phys. Chem.* **98**, 2999 (1994).
42. Gao, X., and Wachs, I. E., *J. Phys. Chem. B* **104**, 1261 (2000).